Active tip deflection control for wind turbines

Liew, Jaime; Lio, Wai Hou; Urbán, Albert Meseguer; Holierhoek, Jessica; Kim, Taeseong

DOI
10.1016/j.renene.2019.12.036

Publication date
2020

Document Version
Final published version

Published in
Renewable Energy

Renewable Energy 149 (2020) 445–454

Contents lists available at ScienceDirect

Renewable Energy

journal homepage: www.elsevier.com/locate/renene

Active tip deflection control for wind turbines

Jaime Liew [a], Wai Hou Lio [a], Albert Meseguer Urbán [a], Jessica Holierhoek [b], Taeseong Kim [a, c, *]

[a] Department of Wind Energy, Technical University of Denmark (DTU), Frederiksborgvej 399, 4000, Roskilde, Denmark
[b] Department of Wind Energy, Delft University of Technology, Delft, the Netherlands
[c] Centre for Renewable Energy Systems Technology (CREST), Wolfson School of Mechanical, Electrical and Manufacturing Engineering, Loughborough University, Loughborough, LE11 3TU, UK

ARTICLE INFO

Article history:
Received 4 March 2019
Received in revised form
22 November 2019
Accepted 8 December 2019
Available online 18 December 2019

Keywords:
Wind energy
Tip deflection sensors
Individual pitch control
Tower clearance
Fatigue load reduction

2010 msc:
00-01
99-00

ABSTRACT

This paper studies the use of blade tip sensors for load reductions and blade-tower clearance control. Typically, modern blade tip sensors measure flapwise tip deflection distances at a high sampling rate, and such measurements can be utilised as feedback signals for control operations. Thus, this paper proposes a novel blade pitch control design based on the tip deflection measurements and individual pitch control (IPC). Firstly, an IPC system design is presented, using the tip deflection measurements to alleviate turbine fatigue loads caused by differential loads such as wind shear, yaw misalignment and turbulence. Secondly, a novel implementation of IPC with tip trajectory tracking feature is proposed where the blade tips are guided along a fixed trajectory to maximise blade-tower clearance. The motivation of this implementation is to reduce the chance of blade-tower interactions for large and flexible rotors. The presented controller is implemented in HAWC2, and high fidelity load measurements are produced using the DTU10MW reference wind turbine. The simulation results showed that the fatigue damage reduction on key turbine components and the improved blade-tower clearance can be achieved simultaneously. Lifetime equivalent load reductions were seen in both rotating and fixed frame components under the normal operating conditions.

1. Introduction

Wind energy technology has seen remarkable growth in recent decades and continues to push boundaries in efficiency and levelised cost of energy. In the battle to reduce the cost of energy, turbine rotors are being upscaled with larger, lighter, and more flexible designs. Two major constraints of modern turbine design are component fatigue stress and blade-tower clearance, both of which become more significant for larger turbine designs. As the blades sweep through the air, large differential forces are experienced in the blade roots and the rotor shaft [1]. The resulting stresses, caused by wind shear, tower shadow, yaw misalignment, nacelle tilt and turbulence, result in accumulated fatigue damage, and can reduce the operating lifetime of the turbine components [2].

Although these differential loads have been thoroughly investigated in literature, the control systems used in modern wind turbines are typically designed with the assumption of uniform blade loading across the rotor plane. Specifically, collective pitch control (CPC) is the standard approach to regulate rotor speed and power output above rated wind speeds despite being ineffective at alleviating blade loads. This is the motivation behind individual pitch control (IPC), where each blade is subject to a different pitch angle depending on the rotational position of the rotor.

The IPC is typically achieved through feedback control using strain gauge measurements. For a standard large-scale three-bladed turbine, strain gauge measurements from each of the three blades are periodic/rotating. It is often that in the literature [3,4], Coleman transformations [5] are employed to simplify the linear blade dynamic model mapping the blade pitch to the blade load measurements. By doing so, the control problem becomes linear time-invariant, and standard proportional-integral (PI) control can be easily performed to balance the loading over the rotor and thus reduce fatigue loads. This transformation technique was originated from the field of helicopter rotor control [5] and similar methods such as direct-quadrature transformation were also widely studied

* Corresponding author. Department of Wind Energy, Technical University of Denmark (DTU), Frederiksborgvej 399, 4000, Roskilde, Denmark.
E-mail addresses: tkim@dtu.dk, aeroelasticwind@gmail.com (T. Kim).

https://doi.org/10.1016/j.renene.2019.12.036
0960-1481/

Nomenclature

ψ	Rotor azimuth angle [rad]
θ_i	Pitch angle of the ith blade [deg]
$\overline{\theta}$	Collective pitch demand [deg]
$\tilde{\theta}_i$	Individual pitch control demand of the ith blade [deg]
y_i	Flapwise tip deflection of ith blade [m]
$\overline{y}$	Mean flapwise tip deflection [m]
$\tilde{y}_i$	Flapwise tip deflection purturbation of the ith blade [m]
$d(t)/d(s)$	Disturbance signal [rad]
$P(s)$	Blade pitch angle to tip deflection transfer function [m/rad]
$C(s)$	Controller transfer function [rad/m]
$F(s)$	Precompensator transfer function [−]
$S(s)$	Sensitivity function [rad/m]
$T(s)$	Complimentary Sensitivity function [rad/m]
K_p	Proportional gain
a	Lead compensator shape constant
T	lead compensator time constant
$r(t)/r(s)$	Target tip deflection reference signal [m]
$\tilde{r}(t)/\tilde{r}(s)$	Compensated target tip deflection reference signal [m]
A_r	Target reference signal amplitude [m]
α	Tip deflection reference signal scale factor [−]
β	Tip deflection reference signal phase shift [rad]
f_{np}	n times per revolution frequency [rad/s]
L_{lt}	Lifetime equivalent load [kNm]

in the field of electrical machines and power electronics [6]. In the field of wind energy control, Coleman-transformed IPC has been widely studied over the past two decades (e.g. Refs. [7–10]) and some successful field tests of Coleman-transformed IPC implementation have been reported [11,12]. Nonetheless, there also exist many variations of IPC design in the literature. For example, the work by Ref. [13] proposed a single blade control architecture, where each blade is equipped with its own controller and transformations are not required. The authors in Ref. [14] suggested another control architecture where Clarke transformations are employed. In this work, we utilise the single blade control architecture.

Often in the literature, the IPC strategies focus mainly on load reductions and little attention is placed on the effect on blade-tower clearance. In particular, the IPC, which only focuses on blade loads, tends to deteriorate the blade-tower clearance, resulting in a reduction of the margin of safety required to avoid tower strikes, which is of particular importance for large rotors [15].

The key contribution of this paper is to tackle this shortcoming in IPC. Specifically, we propose a modified control strategy that not only can reduce the fatigue damage on the blade and other key turbine components, but also can actively increase blade-tower clearance. This is achieved by introducing a reference signal which the controller tracks in addition to minimising oscillations in the blade. By doing so, the controller is able to achieve both fatigue load reductions and increased tower clearance.

The remainder of the paper is structured as follows. In Section 2, the background on IPC and control architecture are presented. Section 3 outlines the HAWC2 simulation setup. In Section 4, the wind turbine model is determined using system identification methods. In Section 5, the proposed IPC design for load reductions and blade-tower clearance is presented and tuned based on the identified turbine model. The performance of the controller in achieving reduced fatigue loads and increased tower clearance is evaluated in Section 6. It is followed by conclusions in Section 7.

2. Background on IPC and control architecture

In general, the IPC system is implemented by superimposing the IPC pitch demands over the pitch demands of the collective pitch controller (CPC), shown in Fig. 1 [16–18]. It is important that the IPC, which is designed for load reduction and increased tower clearance, is decoupled from the CPC whose purpose is to regulate the power output and rotor speed variation above rated wind speeds. In Fig. 1, the individual pitch control system operates with purturbations only ($\tilde{\theta}$ and $\tilde{y}$). Thus, the decoupling is performed by ensuring the mean of the three IPC pitch demands is zero. This ensures there is minimal influence on the power output of the turbine. Consequently, the blade pitch angles and the blade tip deflections are defined in terms of a mean and a purturbation term:

$$\theta_1(t) = \overline{\theta}(t) + \tilde{\theta}_1(t), \tag{1a}$$

$$\theta_2(t) = \overline{\theta}(t) + \tilde{\theta}_2(t), \tag{1b}$$

$$\theta_3(t) = \overline{\theta}(t) + \tilde{\theta}_3(t), \tag{1c}$$

$$y_1(t) = \overline{y}(t) + \tilde{y}_1(t), \tag{1d}$$

$$y_2(t) = \overline{y}(t) + \tilde{y}_2(t), \tag{1e}$$

$$y_3(t) = \overline{y}(t) + \tilde{y}_3(t), \tag{1f}$$

where

$$\overline{\theta}(t) = \frac{1}{3}\sum_{i=1}^{3}\theta_i(t), \tag{1g}$$

$$\overline{y}(t) = \frac{1}{3}\sum_{i=1}^{3}y_i(t), \tag{1h}$$

and $\overline{\theta}$ and $\overline{y}$ represent the CPC pitch demand and the mean tip deflection respectively.

The relationship between the perturbation in the blade pitch angle $\tilde{\theta}_i$ and blade tip displacement $\tilde{y}_i$ can be modelled by a transfer function $P(s)$, that is obtained by linearising the turbine dynamics about the rated rotor speed and an operating wind speed. In Fig. 2, the control-oriented linear model of the blade tip dynamics $P(s)$ is presented with feedback interconnected with the linear controller $C(s)$.

As the IPC controls all three turbine blades simultaneously, it is common for a system transformation to be performed in order to simplify the control system. This study uses single blade control instead of the more commonly used Coleman transformation based control [17]. This method has the advantage of being simple to implement and assumes each blade is uncoupled. For a three bladed turbine, three identical single-input single-output (SISO) controllers can be cascaded to determine the pitch demands (Fig. 3). Additionally, the controller does not require the rotor azimuth angle as a measurement. Single blade control has been

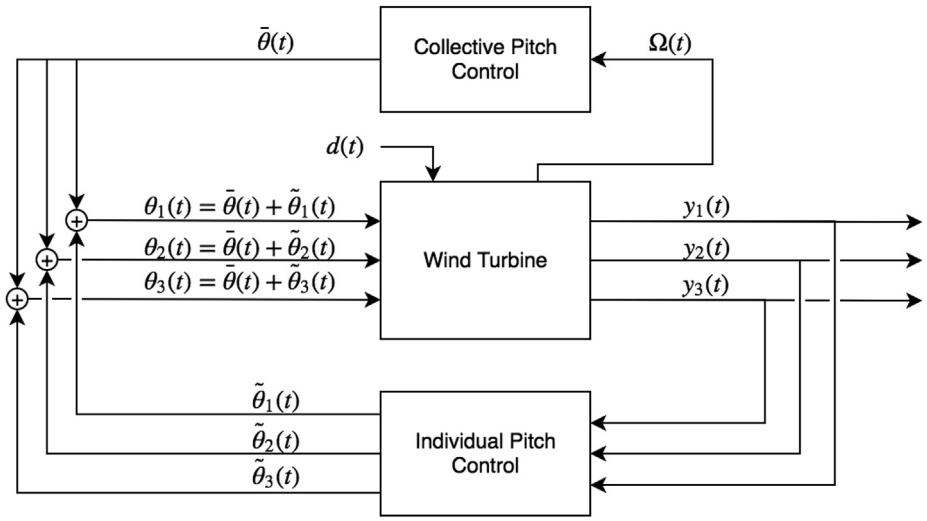

Fig. 1. Block diagram of wind turbine control architecture with both collective pitch control (CPC) and individual pitch control (IPC). The CPC regulates rotor speed while the IPC attenuates flapwise tip deflection perturbations as well as increasing tower clearance. Additional inputs to the turbine, such as wind loading and generator torque, are accounted for in the term $d(t)$.

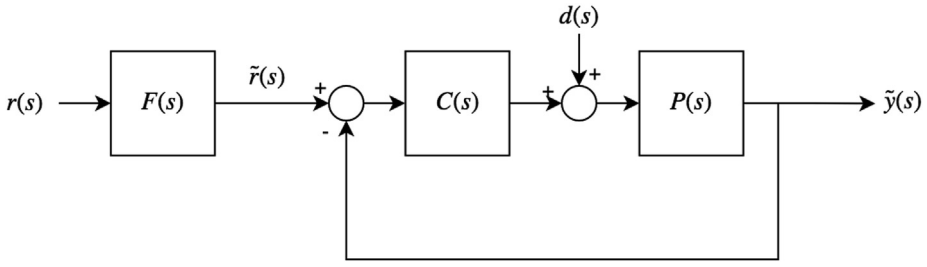

Fig. 2. Linear block diagram representing the feedback interconnection between the blade pitch angle to tip deflection system ($P(s)$) and the IPC controller ($C(s)$) for a single blade.

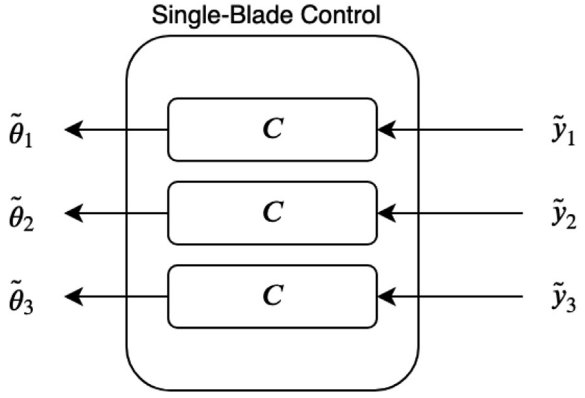

Fig. 3. Single blade transform block diagram. The pitch demand for each blade, $\tilde{\theta}_i$, is determined only from the measurement of that blade, $\tilde{y}_i$.

successfully implemented in simulation in Refs. [13,19].

The use of single blade control over Coleman transform-based control is justified on a theoretical basis. The Coleman transform transforms the stresses or tip deflection measurements from the rotating frame of reference to the stationary frame of reference. When used in a control system, the measurements for the three blades are decomposed into a tilt and yaw component, where the control action is performed. Coleman transform-based control typically assumes the tilt and yaw axes are decoupled, which can cause problems in the control design. Lu et al. [16] provides a mathematical formulation of the tilt-yaw coupling, showing that the assumption that tilt and yaw are decoupled does not hold in certain scenarios and therefore requires further attention in the control design process. Furthermore, the transformation itself is nonlinear, causing a frequency shift in the transformed domain. In particular, the f_{1p} blade loads are shifted to f_{0p} and f_{2p} in the fixed frame. Similarly, f_{3p} oscillations in the fixed frame manifest themselves as f_{2p} and f_{4p} oscillations in the rotating frame [16,18,20]. These effects can cause poor control performance if they are not taken into account in the design process.

To overcome these issues, single blade control (Fig. 3) is performed instead. It is shown in Ref. [20] that a single blade control law can be converted to an equivalent Coleman transform-based control law, and that these equivalent controllers yield identical performance. The advantage of designing the controller in this way is that the converted single blade controller already takes into account the effects tilt-yaw coupling, which is often overlooked in Coleman transform-based control design. For this reason, it is chosen to explore the single blade control which treats each blade as an independent system. Each individual blade with IPC can be modelled as the closed loop system shown in Fig. 2.

3. Simulation setup

The aeroelastic code HAWC2, which is able to simulate wind turbine responses in the time domain, is used in this study. HAWC2 is able to couple the turbine structural dynamics, the aerodynamic forces from the wind, and the control system to produce high

fidelity simulation data [21–23]. Multi-body beam elements are used to model the structure of the turbine. The rotor aerodynamics is calculated using a blade element momentum theory formulation, and the turbulence is generated using the Mann turbulence model [24]. Time series data of the bending moments of various components, tip deflection of the blades, and blade pitch angle signals are collected and analysed in this work to evaluate and verify the effectiveness of the IPC control system.

The DTU10MW Reference Wind Turbine Model is used in this study for the design and testing of the control systems [25]. The standard controller used for this turbine is the Basic DTU Wind Energy controller described in Ref. [26]. The IPC controllers analysed in this study are designed to extend the standard controller. Some of the key specifications used in this study are tabulated in Table 1.

During the lifetime of a wind turbine, the most frequent operation conditions are the normal operation condition under the normal turbulence. This is defined in the IEC 61400 standards as DLC1.1 and DLC1.2 for ultimate load and fatigue load analysis, respectively [27]. Therefore, DLC1.2 is selected for this paper in order to analyze the controller performance related to the fatigue load and blade-tower clearance.

4. System identification of the blade tip dynamics

In order to design the IPC, a linearised model of the transfer function, $P(s)$ is first determined. $P(s)$ encapsulates the dynamics between the pitch angle demand of a single blade and the flapwise tip deflection of the blade, and therefore includes the dynamics from the pitch actuator, blade structure, aerodynamic forces and the tip deflection sensor itself. The transfer function estimation is performed in Matlab [28] using the time series data plotted in Fig. 4, which are the response of the blade tip displacement at varying wind speeds (lower plots) to a step change in blade pitch input (upper plot) given that the turbine is operating at the steady-state. Further simplifications are also made by assuming no wind shear, tower shadow, turbulence or nacelle tilt to isolate the effect of pitch angle on blade tip deflection. The time series input and output are run through the spafdr function (spectral analysis with frequency-dependent resolution) to obtain an estimate for the frequency response of each time series. This allows the system identification to be performed in the frequency domain, which provides a smoother and more consistent transfer function than the time domain system identification methods. The spafdr function uses a similar method outlined by Ljung [29]. First, the autospectrum of the discrete input signal, $\Phi_{xx}(\omega)$, as well as the cross spectrum, $\Phi_{xy}(\omega)$ are estimated. The frequency response of black-box system, $P(z)$ is estimated as:

$$P\left(e^{j\omega}\right) = \frac{\Phi_{xy}(\omega)}{\Phi_{xx}(\omega)}. \tag{2}$$

The estimated frequency response is run through the tfest function to find the best fitting transfer function coefficients. The tfest is able to estimate a continuous-time transfer function given a discrete frequency domain input and output signal using quadrature-based vector fitting [30]. Among the various transfer function structures tested, a transfer function with four poles and three zeros was found to fit most appropriately, defined as follows:

$$P(s) = \frac{-11.93s^3 + 23.92s^2 + 1621.75s + 1018.02}{s^4 + 4.91s^3 + 27.69s^2 + 35.08s + 29.14}. \tag{3}$$

Fig. 5 shows the bode plot corresponding to the fitted plant transfer functions for various wind speeds. The system behaves similar to a low pass filter, implying that high frequency pitching is attenuated due to the system dynamics. It can also be seen that the blade models in the above rated wind speed closely match, that implies a gain-scheduling design might not be necessary. In contrast, the model in the below rated wind speed shows some deviations, which is a result of the changing turbine dynamics due to the varying rotor speed. A separate design is needed for the below rated wind speed conditions.

Table 1
DTU10MW reference wind turbine model key parameters.

Parameter	Value
Wind regime	IEC Class 1A
Rated power output	10 MW
Rated wind speed	11.4 m/s
Rotor diameter	178.3m
Hub height	119.0m
Minimum rotor speed	6 RPM (0.1 Hz)
Rated rotor speed	9.6 RPM (0.16 Hz)

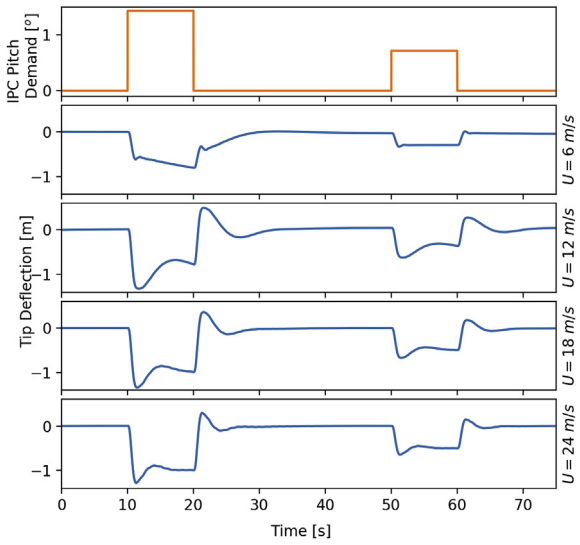

Fig. 4. Time series of IPC pitch demand (top figure) and their corresponding flapwise tip deflection perturbation response at various wind speeds.

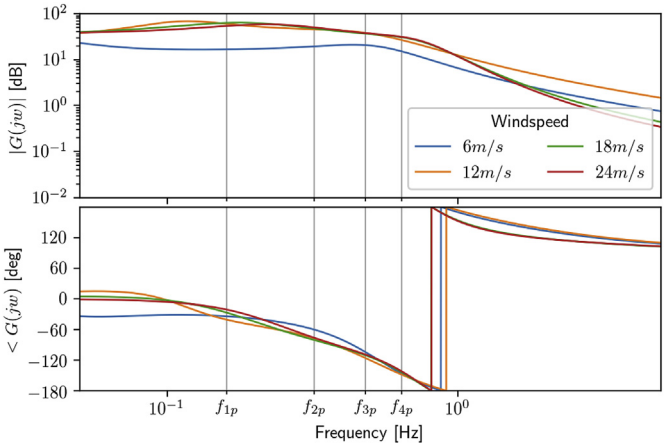

Fig. 5. Bode plot of fitted transfer functions between IPC pitch demand and flapwise tip deflection purturbation at varying wind speeds.

5. Control design

5.1. Load reductions

Each blade is fitted with an independent and identical pitch controller and precompensator, $C(s)$ and $F(s)$ as shown in Fig. 2. The controller $C(s)$ is designed for disturbance rejection by ensuring frequency components with the largest contribution to fatigue loads are not passed through the system. This is achieved with loop shaping to minimise the sensitivity function $S(s)$ at key frequencies while maintaining a minimum stability margin. The sensitivity function $S(s)$ is defined as follows:

$$S(s) = \frac{1}{1 + P(s)C(s)}. \tag{4}$$

Load reductions in both rotating components (i.e. blades) and non-rotating components (main bearing, tower, etc.) are achieved by attenuating flapwise blade tip deflection fluctuations which modulate at both *once per revolution* (f_{1p}) and *twice per revolution* (f_{2p}) frequencies. f_{1p} fluctuations (1.005 rad/s) are significant to blade loads, whereas f_{2p} fluctuations contribute to fixed-frame component loads as the oscillation is modulated to a load at f_{3p} in the fixed frame. Higher order oscillations are not considered as the majority of the fluctuation energy is concentrated at f_{1p} and f_{2p} frequencies, and to avoid exceeding pitch rate limits of the pitch actuator.

The IPC utilises the transfer function $C(s)$, as defined in Equation (5), consisting of two band pass filters and two identical lead compensators, defined as follows:

$$C(s) = K_p \left(\frac{s^2 + 2\zeta_1\omega_1 s + \omega_1^2}{s^2 + 2\zeta_2\omega_2 s + \omega_2^2} \right) \left(\frac{s^2 + 2\zeta_3\omega_3 s + \omega_3^2}{s^2 + 2\zeta_4\omega_4 s + \omega_4^2} \right) \left(\frac{1 - aTs}{1 - Ts} \right)^2. \tag{5}$$

The band pass filters with the parameters ω_i and ζ_i for $i = 1, 2, 3, 4$, are tuned to target the f_{1p} and f_{2p} frequencies. To compensate for the lag introduced by the band pass filters, two identical lead compensators, with shape and time parameters, a and T, are included. a, T, as well as the proportional gain, K_p, are tuned using loop shaping techniques to ensure closed loop robustness and adequate attenuation of the target frequencies [31]. Consequently the gain of the systems sensitivity function $S(s)$, mapping $d(s)$ to $\tilde{y}(s)$ in Fig. 7, is tuned to be particularly low at the f_{1p} and f_{2p} frequencies. The lead compensator parameters are chosen to maximise the stability margin $s_m(P, C)$ defined as the minimum distance between the Nyquist plot of the feedback system and the critical point, $s = -1$ [32]:

$$s_m(P(s), C(s)) = \min_{\omega} |P(j\omega)C(j\omega) + 1|. \tag{6}$$

The parameters used for the controller, $C(s)$, are listed in Table 2.

5.2. Blade-tower clearance

The main principle behind increasing tower clearance is to guide the blade tips along a preset trajectory. This is essentially a tracking problem. Tracking problems in a single-input-single-outing (SISO) system typically can be solved by employing a simple proportional-integral (PI) feedback control design. However, in this study, the IPC feedback controller is constructed in a way to attenuate the blade loads at f_{1p} and f_{2p} frequencies. The tracking feature is then added on the pre-determined closed-loop system. Thus, it is critical to design the precompensator $F(s)$ carefully.

The transfer function of the precompensator, $F(s)$, is designed such that the tip deflection output tracks the reference signal, $r(s)$. To demonstrate this concept, consider Fig. 6, which shows an example of the target tip deflection reference signal and the compensated reference signal for each blade, where the blue lines represent the desired tip deflection trajectory for a single blade as a function of rotor azimuth angle. The desired trajectory is a sinusoid with a f_{1p} frequency such that the peak is located at the azimuth angle where the blades are pointing downwards as to maximise tower clearance, defined as follows:

$$r_1(t) = A_r \cos(\psi(t)), \tag{7a}$$

$$r_2(t) = A_r \cos\left(\psi(t) + \frac{2\pi}{3}\right), \tag{7b}$$

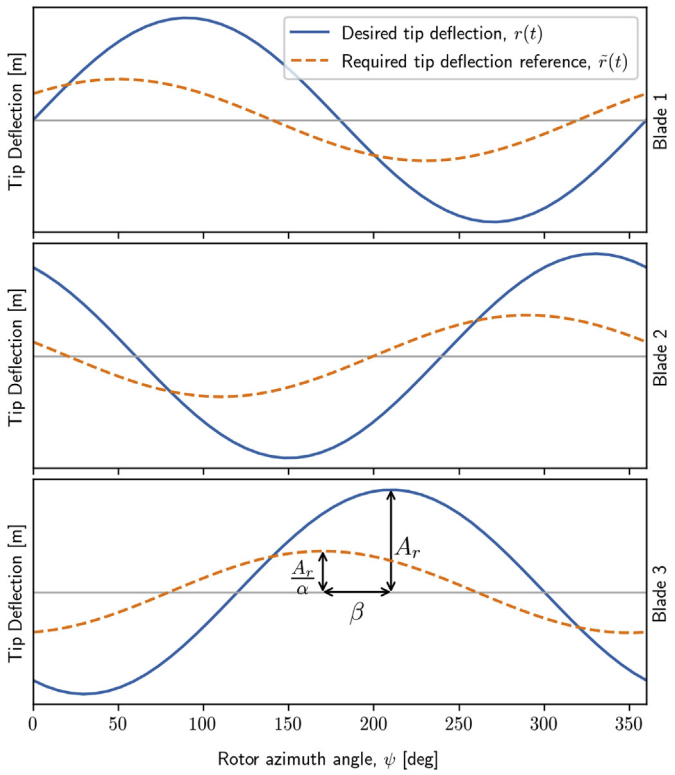

Fig. 6. Example of the target tip deflection reference signal, $r(t)$, and the compensated reference signal, $\tilde{r}(t)$ for each blade.

Table 2
The parameters for the IPC controller $C(s)$.

K_p	ω_1	ω_2	ω_3	ω_4	
0.043	0.955 rad/s	1.568 rad/s	2.010 rad/s	3.016 rad/s	
ζ_1	ζ_2	ζ_3	ζ_4	a	T
0.15	0.1	0.1	0.3	13.928	0.267

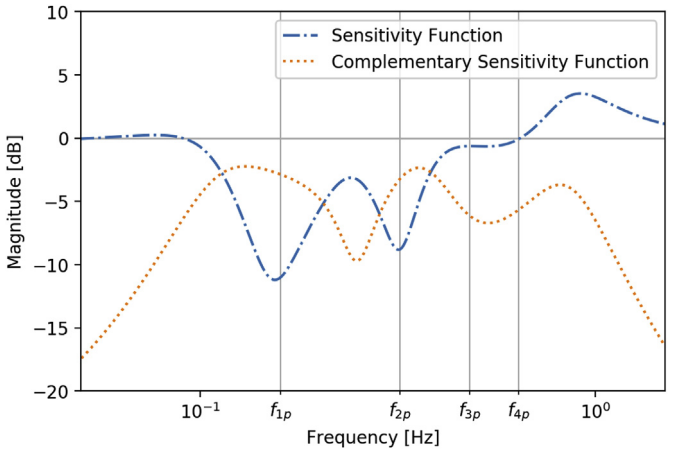

Fig. 7. Magnitude plot of sensitivity function, $S(s)$, and complimentary sensitivity function, $T(s)$ corresponding to the closed loop IPC system ($F(s) = 1$).

$$r_3(t) = A_r \cos\left(\psi(t) + \frac{4\pi}{3}\right), \tag{7c}$$

where ψ denotes the rotor azimuth angle, and $r_i(t)$ the reference signal of the ith blade. The amplitude of the desired tip deflection trajectory represented by the value A_r is chosen arbitrarily to introduce the desired amount of tower clearance. To achieve this desired trajectory, a compensated reference signal, $\tilde{r}(t)$ is subjected to the control loop, shown by the orange dashed line in Fig. 6. The compensated reference signal has a phase lead, β, and a scaling factor, α, relative to the desired tip deflection trajectory. The compensated reference signals are defined as follows:

$$\tilde{r}_1(t) = \frac{A_r}{\alpha}\cos(\psi(t) - \beta), \tag{8a}$$

$$\tilde{r}_2(t) = \frac{A_r}{\alpha}\cos\left(\psi(t) + \frac{2\pi}{3} - \beta\right), \tag{8b}$$

$$\tilde{r}_3(t) = \frac{A_r}{\alpha}\cos\left(\psi(t) + \frac{4\pi}{3} - \beta\right). \tag{8c}$$

The values of α and β are determined by tuning $F(s)$ from the complementary sensitivity function such that the gain and phase of the output matches the gain and phase of the reference signal. As the reference signal is a sinusoidal oscillating at a frequency of f_{1p}, it is sufficient to design $F(s)$ such that only f_{1p} frequency components are compensated correctly. By doing so, it is assumed that $F(s)$ is a constant with a complex value.

Consider the transfer function between the reference signal, $r(s)$ and the tip deflection, $\tilde{y}(s)$, also known as the complimentary sensitivity function, $T(s)$.

$$T(s) = \frac{\tilde{y}(s)}{r(s)} = F(s)\frac{P(s)C(s)}{1 + P(s)C(s)}. \tag{9}$$

Fig. 7 shows that the magnitude of the complimentary sensitivity function $T(s)$ is less than 1 (or 0 dB), implying that the controller would not be able to track a reference signal $r(t)$ at the frequency f_{1p} if $F(s) = 1$. To ensure the output tracks the reference, the complimentary sensitivity function $T(s)$ needs to be 0 dB magnitude with phase of 0° at that frequency. Thus, to find the right precompensator $F(s)$ at frequency f_{1p}, The complimentary sensitivity function $T(s)$ was set to 1 in left hand side of Equation (9).

Evaluating the right hand side of Equation (9) at the reference signal frequency ($s = j2\pi f_{1p}$) yields:

$$1 = F\left(j2\pi f_{1p}\right)\alpha e^{j\beta}, \tag{10}$$

where α and β are real numbers and $ae^{j\beta}$ is a known complex number in exponential form such that

$$\alpha e^{j\beta} = \frac{P\left(j2\pi f_{1p}\right)C\left(j2\pi f_{1p}\right)}{1 + P\left(j2\pi f_{1p}\right)C\left(j2\pi f_{1p}\right)}. \tag{11}$$

The values of α and β can be obtained directly from Fig. 7 α equals the magnitude at f_{1p}, and β equals the phase at f_{1p}.

Rearranging Equation (10) yields:

$$F\left(j2\pi f_{1p}\right) = e^{-j\beta} \Big/ \alpha. \tag{12}$$

If this condition is true, then $y(s)$ will track $r(s)$ with the same magnitude and phase. Specifically, $\alpha = 1/\left|T(f_{1p})\right|$ and $\beta = \angle(T(f_{1p}))$. Hence $\tilde{r}(t)$ can be explicitly defined as a function of rotor azimuth in Equation (8).

6. Results

6.1. Disturbance rejection

The controller is initially implemented with no tip trajectory tracking (TTT) ($A_r = 0m$) to represent an IPC designed for disturbance rejection only. Fig. 8 shows the frequency sensitivity of the simulated results over all operating wind speeds. In this figure, the contours represent the change in tip deflection magnitude for a given wind speed and frequency component as a result of using IPC. The tip deflection magnitudes are determined by performing the discrete Fourier transform on the tip deflection time series data.

The controller is successfully able to attenuate f_{1p} and f_{2p} tip deflection oscillation amplitudes above the rated wind speed of $11.4m/s$ (by 67.88% and 59.00% respectively at $U = 18m/s$). The attenuated frequency bands correspond to the sensitivity function of the controller shown in Fig. 7. A slight amplification in frequencies above f_{4p} can also be observed, and is also predicted from the sensitivity function. This amplification is an unavoidable

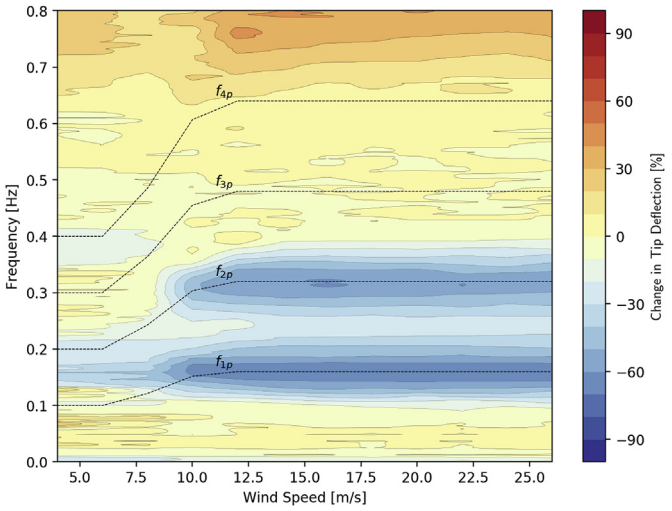

Fig. 8. Change in tip deflection magnitude as a function of wind speed and frequency from HAWC2 simulations.

consequence of Bode's theorem, which states the integral of the logarithmic magnitude of a sensitivity function is zero for a single-input single-output stable system. Therefore, a trade-off must be made between disturbance attenuation in amplification over all frequency ranges [33]. Due to the low energy content in these frequency ranges compared to f_{1p} and f_{2p}, this amplification is considered insignificant with regards to fatigue loads.

The ability of the controller to attenuate f_{1p} and f_{2p} degrades below rated wind speed due to the shift in rotor speed. This is a result of the set frequency response of the controller, which is tuned for the rated rotational frequency. It can be expanded to consider all range of rotor speeds by gain scheduling the controller, which is a topic for future work.

6.2. Tip trajectory tracking

Reference signals with different tracking amplitudes were tested for A_r between $0m$ and $4m$. Fig. 9 shows the tip deflection results of the HAWC2 simulations for the first blade, showing the controller is able to successfully track the reference signal (red dotted line) with comparable phase and amplitude. Although the standard deviation of the tracking error is less than $0.764m$ for the tested values of A_r, it should be noted that the simulations assume an ideal tip deflection sensor. In more realistic settings, the sensor dynamics and noise need to be taken into account in the controller design process.

To better investigate the effects of TTT on tower clearance including effects of blade pitching and tower motion, the minimum passing distance between each blade and the tower is recorded and plotted in Fig. 10 showing the distribution of tower clearance for each passing event. It is interesting to note that the average tower clearances when using standard IPC ($A_r = 0m$) is less than the CPC case alone. The effects of wind shear and tower shadow tend to be beneficial for tower clearance by causing the blades to naturally deflect away from the tower due to the added wind deficit. By introducing IPC, this beneficial effect is counteracted. As a consequence of overcoming these effects, standard IPC controllers tend to decrease tower clearance despite having load reduction capabilities. By introducing TTT with $A_r = 1m$, the tower clearance distributions (minimum and mean) can be increased to the CPC level and beyond. Further increases in A_r cause a corresponding increase in tower clearance.

6.3. Fatigue load reductions

Fatigue loads are quantified using the 1 Hz damage equivalent load which is calculated using the rainflow counting algorithm [34]. A Wöhler exponent of 10 and 4 are used for calculating fatigue loads for the turbine blades and main shaft respectively. By designing the controller to attenuate both f_{1p} and f_{2p} blade oscillations, the turbine experiences lower 1 Hz equivalent fatigue loads in both the blade roots (flapwise) and in the main shaft when no tracking is used ($A_r = 0m$, Fig. 11). These load reductions are most significant above rated wind speeds when comparing to the CPC only case. Further improvements in the below rated region can be achieved with gain scheduling of the controller, as mentioned above. When TTT is introduced, an f_{1p} oscillation in the blades is induced, having the effect of increasing blade fatigues loads. Shown in Fig. 11, the blade fatigue loads increase monotonically with A_r. However, for $A_r \leq 2m$, the 1 Hz equivalent flapwise blade loads are less than the CPC only case, showing that both TTT and load reductions can be achieved simultaneously if A_r is below a threshold value. The lifetime damage equivalent loads, shown in Table 3, are calculated by taking the weighted average of the 1 Hz damage equivalent load, where the weighting is a Weibull distribution ($A = 11.28$, $k = 2$) corresponding to a Class IA wind conditions defined in IEC 61400 [27]. The results confirm that tip trajectory set point of $A_r = 2$ can be set while still maintaining lower blade loads than the CPC case. The shaft load reductions show negligible change due to increases in A_r. This is a benefit of choosing a sinusoidal reference signal with a frequency of f_{1p} as described in Equation (8). The 120^o phase difference in each blade signal results in a load cancellation

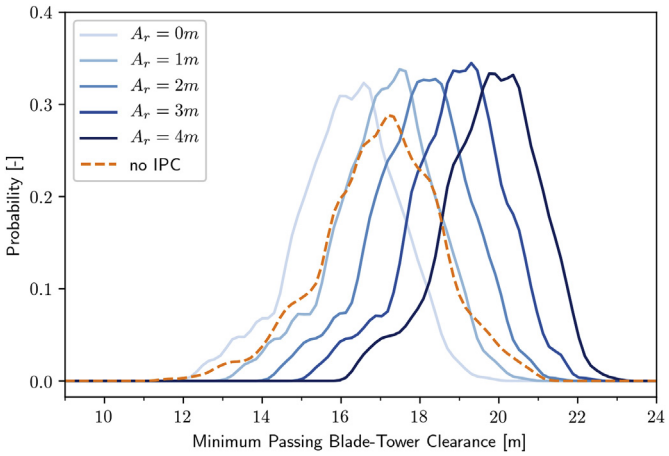

Fig. 10. Probability distribution of minimum passing distance between blade tips and tower (from HAWC2 simulations).

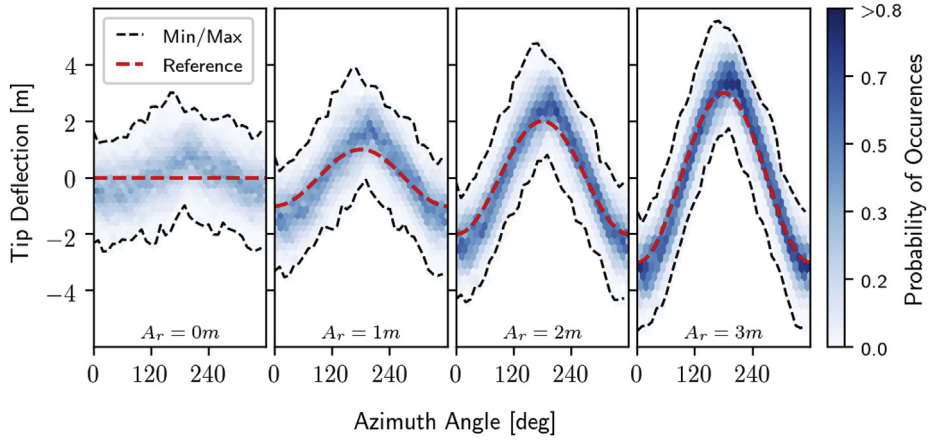

Fig. 9. Flapwise tip deflection perturbation as a function of rotor azimuth angle for varying tip trajectory set points (from HAWC2 simulations).

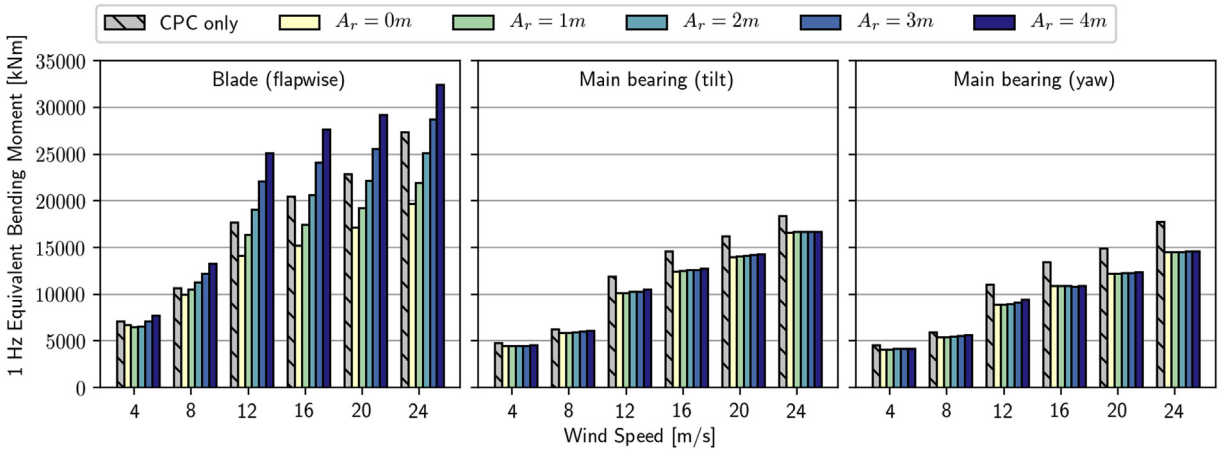

Fig. 11. Fatigue loads of various turbine components for a range of wind speeds and tip trajectory set points.

Table 3
Lifetime equivalent loads, L_{lt}, [kNm] of TTT controller for varying tip trajectory set points. Percent change is based on the CPC case.

	$A_r = 0$		$A_r = 1$		$A_r = 2$		$A_r = 3$		$A_r = 4$	
	L_{lt}	% chng	L_{lt}	% chng	L_{lt}	% chng	L_{lt}	% chng	L_{lt}	% chng
Blade (flap)	13942	−25.10	15744	−15.42	18218	−2.13	20965	+12.63	23872	+28.25
Main Bearing (tilt)	8675	−13.19	8706	−12.89	8762	−12.33	8799	−11.96	8908	−10.87
Main Bearing (yaw)	7636	−17.88	7633	−17.91	7649	−17.73	7680	−17.40	7763	−16.51

between the three blades as the moments are modulated from the rotating frame to the fixed frame of reference. This prevents oscillations in the fixed frames and therefore causes no change to the fixed frame fatigue loads.

Despite the reduced blade and main shaft loads, it is important to consider the corresponding effect on pitch activity and pitch bearing loads. In Fig. 12, the pitch rate probability distribution and the blade root torsion equivalent load are shown as a representation of pitch bearing activity and fatigue loads. The blade root torsion equivalent loads show a similar pattern to that of the blade flapwise loads, where values of A_r less than 2 show a load decrease. Large values of A_r show a significant increase in loads, especially near rated wind speed. The pitch rate probability distribution is shown for a wind speed of 12 m/s to represent the most sever case which occurs near rated wind speed, and demonstrates that the pitch rate remains within the limit suggested by Ref. [2] of $10^o/s$.

6.4. Effect on annual energy production (AEP)

The AEP is estimated by taking the weighted average of power production over the operating wind speeds, where the weighting is the same Weibull distribution used in the lifetime equivalent load calculations above. Theoretically, IPC has no impact on the power output of a wind turbine. This is a result of the decoupling between the IPC and the CPC by ensuring $\tilde{\theta}_1(t) + \tilde{\theta}_2(t) + \tilde{\theta}_3(t) = 0$. In practice, there are discrepancies in the wind field and turbine dynamics which cause a decrease in AEP as A_r is increased. Tabulated in Table 4, it can be seen that AEP tends to decrease for larger values of

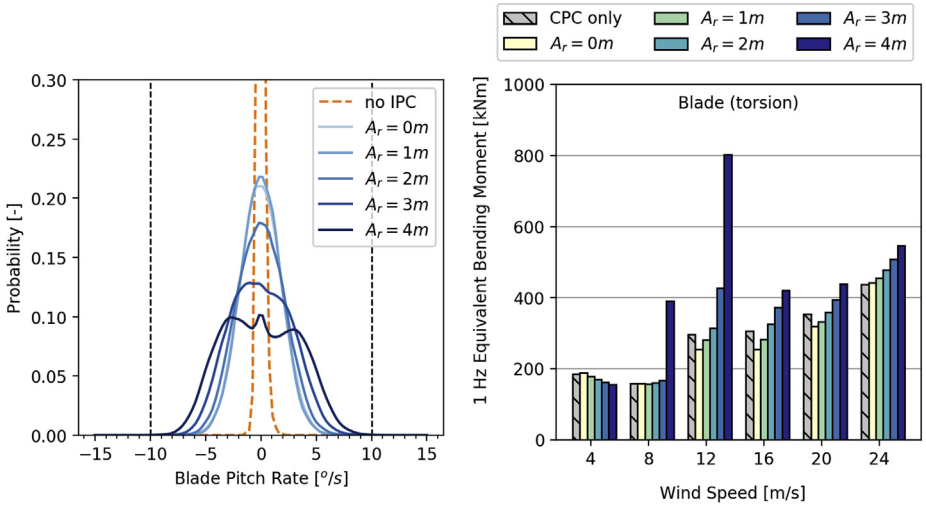

Fig. 12. Left: Blade pitching rate probability distribution (ind speed = $12m/s$). Right: Blade root torsion damage equivalent loads for varying tip trajectory set points.

Table 4
Change in AEP for varying tip trajectory set points, assuming TTT is activated at all times.

Controller	CPC only	CPC and TTT				
		$A_r = 0m$	$A_r = 1m$	$A_r = 2m$	$A_r = 3m$	$A_r = 4m$
Change in AEP	0.00%	−0.39%	−0.23%	−0.31%	−0.68%	−1.35%

A_r. This is also the case for standard IPC ($A_r = 0$). It should be noted that the AEP calculations assume that the IPC is active at all times, and therefore the reduction in AEP may be less significant if the IPC is active during high risk periods only.

7. Conclusions

The key contribution of this paper is to propose an individual pitch control (IPC) strategy based on tip deflection sensors. Such a strategy can reduce the fatigue load on the blade and other key turbine components, while actively increasing the blade-tower clearance. Specifically, the novel IPC design is constructed based on a linear blade tip deflection model estimated using system identification techniques. The IPC is then tuned to target the key load frequencies f_{1p} and f_{2p}, in order to achieve load reductions in both rotating and non-rotating turbine components. Furthermore, the proposed IPC is modified to increase the blade-tower clearance. The key to this modification is that the reference signal is adjusted with the compensated magnitude and phase. High fidelity simulations upon a non-linear turbine model (DTU10MW) showed the proposed control method achieved significant load reductions whilst maintaining an increase of 2m in the minimal distance between the blade-tip and tower over the operating wind conditions.

The presented controller is relevant in wind turbine design optimisation, where it could be possible to reduce the rotor mass, cone angle and tilt angle while maintaining a safe blade-tower clearance distance by using active tip deflection control. Alternatively, the blade length can be extended to increase the rotor area, resulting in higher annual energy production. The potential decrease in levelised cost of energy must be weighed against the increased pitch activity required to perform tip deflection control, and is a topic for future research work.

Author contribution statement

Jaime Liew: Methodology, Writing original draft preparation, visualization, Investigation, Formal analysis

Wai Hou Lio: Supervision, Investigation, Writing, Reviewing and Editing

Albert Meseguer Huran: Software, Investigation, Writing, Reviewing and Editing

Jessica Holierhoek: Supervision, Investigation, Writing, Reviewing and Editing

Taeseong Kim: Supervision, Investigation, Writing, Reviewing and Editing, Project administration

Declaration of competing interest

The authors declare that they have no known competing financial interests or personal relationships that could have appeared to influence the work reported in this paper.

Acknowledgement

The authors wish to acknowledge Christian Frank Andersen and Armin Hermes from LM Wind Power for their valuable input and support. This work was supported by the Korea Institute of Energy Technology Evaluation and Planning (KETEP), the Ministry of Trade, Industry & Energy (MOTIE) of the Republic of Korea (no. 20168520021200), and the Korea Institute of Energy Research (KIER) (B9-2463-05).

References

[1] S. Kanev, T. van Engelen, Wind turbine extreme gust control, Wind Energy 13 (1) (2010) 18–35.
[2] E. Bossanyi, A. Ervin, The design of closed loop controllers for wind turbines, Wind Energy 3 (3) (2000) 149–163.
[3] E.A. Bossanyi, Wind turbine control for load reduction, Wind Energy 6 (3) (2003) 229–244.
[4] T.G. van Engelen, Design model and load reduction assessment for multi-rotational mode individual pitch control (higher harmonics control), in: Proc. of European Wind Energy Conference, 2006.
[5] R. P. Coleman, A. M. Feingold, Theory of Self-Excited Mechanical Oscillations of Helicopter Rotors with Hinged Blades.
[6] P. Vas, Electrical Machines and Drives: a Space-Vector Theory Approach, Oxford University Press, 1992.
[7] K. Selvam, S. Kanev, J.W. van Wingerden, T. van Engelen, M. Verhaegen, Feedback-feedforward individual pitch control for wind turbine load reduction, Int. J. Robust Nonlinear Control 19 (1) (2009) 72–91, https://doi.org/10.1002/rnc.1324.
[8] C. Bottasso, A. Croce, C. Riboldi, Y. Nam, Multi-layer control architecture for the reduction of deterministic and non-deterministic loads on wind turbines, Renew. Energy 51 (2013) 159–169, https://doi.org/10.1016/j.renene.2012.08.079. http://linkinghub.elsevier.com/retrieve/pii/S0960148112005691.
[9] C. Plumley, W. Leithead, P. Jamieson, E. Bossanyi, M. Graham, Comparison of individual pitch and smart rotor control strategies for load reduction, in: Proc. of the Science of Making Torque from Wind 524, 2014, 012054.
[10] S.T. Navalkar, J.W. van Wingerden, G.a.M. van Kuik, Individual blade pitch for yaw control, J. Phys. Conf. Ser. 524 (2014), 012057, https://doi.org/10.1088/1742-6596/524/1/012057. http://stacks.iop.org/1742-6596/524/i=1/a=012057?key=crossref.2de02c0a9cb6cfff389604dd29216a38.
[11] E.A. Bossanyi, A. Wright, Field testing of individual pitch control on the NREL CART-2 wind turbine, in: European Wind Energy Conference, 2009.
[12] E.A. Bossanyi, P.A. Fleming, A.D. Wright, Validation of individual pitch control by field tests on two- and three-bladed wind turbines, IEEE Trans. Control Syst. Technol. 21 (4) (2013) 1067–1078, https://doi.org/10.1109/TCST.2013.2258345. http://ieeexplore.ieee.org/lpdocs/epic03/wrapper.htm?arnumber=6515638.
[13] W. Leithead, V. Neilson, S. Dominguez, A. Dutka, A novel approach to structural load control using intelligent actuators, in: Control and Automation, 2009. MED'09. 17th Mediterranean Conference on, IEEE, 2009, pp. 1257–1262.
[14] Y. Zhang, M. Cheng, Z. Chen, Proportional resonant individual pitch control for mitigation of wind turbines loads, IET Renew. Power Gener. 7 (3) (2013) 191–200, https://doi.org/10.1049/iet-rpg.2012.0282.
[15] P.S. Veers, T.D. Ashwill, H.J. Sutherland, D.L. Laird, D.W. Lobitz, D.A. Griffin, J.F. Mandell, W.D. Musial, K. Jackson, M. Zuteck, et al., Trends in the design, manufacture and evaluation of wind turbine blades, Wind Energy: Int. J. Progress Appli. Wind Power Convers. Technol. 6 (3) (2003) 245–259.
[16] Q. Lu, R. Bowyer, B.L. Jones, Analysis and design of coleman transform-based individual pitch controllers for wind-turbine load reduction, Wind Energy 18 (8) (2015) 1451–1468.
[17] E. Bossanyi, Individual blade pitch control for load reduction, Wind Energy 6 (2) (2003) 119–128.
[18] S. Kanev, T. Van Engelen, Exploring the limits in individual pitch control, in: European Wind Energy Conference, 2009, pp. 1–10.
[19] T.J. Larsen, H.A. Madsen, K. Thomsen, Active load reduction using individual pitch, based on local blade flow measurements, Wind Energy 8 (1) (2005) 67–80.
[20] W.H. Lio, B.L. Jones, Q. Lu, J. Rossiter, Fundamental performance similarities between individual pitch control strategies for wind turbines, Int. J. Control 90 (1) (2017) 37–52.
[21] T. J. Larsen, A. M. Hansen, How 2 HAWC2, the User's Manual.
[22] T. Kim, A.M. Hansen, K. Branner, Development of an anisotropic beam finite element for composite wind turbine blades in multibody system, Renew. Energy 59 (2013) 172–183.
[23] T.J. Larsen, H.A. Madsen, G.C. Larsen, K.S. Hansen, Validation of the dynamic wake meander model for loads and power production in the egmond aan zee wind farm, Wind Energy 16 (4) (2013) 605–624.
[24] J. Mann, Wind field simulation, Probabilistic Eng. Mech. 13 (4) (1998) 269–282.
[25] C. Bak, F. Zahle, R. Bitsche, T. Kim, A. Yde, L. Henriksen, M. Hansen, J. Blasques, M. Gaunaa, A. Natarajan, reportDescription of the DTU 10 MW Reference Wind Turbine. DTU Wind Energy Report-I-0092, Technical University of Denmark, Fredericia (Denmark).
[26] M. H. Hansen, L. C. Henriksen, Basic DTU Wind Energy Controller.

[27] International Electrotechnical Commission, IEC 61400-1: Wind Turbines Part 1: Design Requirements, third ed., IEC, 2005.
[28] MATLAB, Version 7.10.0 (R2010a), The MathWorks Inc., Natick, Massachusetts, 2010.
[29] L. Ljung, System Identification: Theory for the User, Prentice-Hall, Inc., Upper Saddle River, NJ, USA, 1986.
[30] Z. Drmac, S. Gugercin, C. Beattie, Quadrature-based vector fitting for discretized h_2 approximation, SIAM J. Sci. Comput. 37 (2) (2015) A625–A652.
[31] D. McFarlane, K. Glover, A loop-shaping design procedure using h/sub infinity/ synthesis, IEEE Trans. Autom. Control 37 (6) (1992) 759–769.
[32] K.J. Aström, R.M. Murray, Feedback Systems: an Introduction for Scientists and Engineers, Princeton university press, 2010.
[33] J. Freudenberg, D. Looze, Right half plane poles and zeros and design tradeoffs in feedback systems, IEEE Trans. Autom. Control 30 (6) (1985) 555–565.
[34] M. Matsuishi, T. Endo, Fatigue of Metals Subjected to Varying Stress, vol. 68, Japan Society of Mechanical Engineers, Fukuoka, Japan, 1968, pp. 37–40, 2.